TEKNILLINEN KORKEAKOULU
Teknillisen fysiikan koulutusohjelma

ERIKOISTYÖ
Tfy-56.198 Energiateknologiat
1.10.2002

NUMERICAL STUDIES ON SONOLUMINESCENCE

Mikko Voutilainen
51693R

Contents

1 Introduction **2**
1.1 Sonoluminescence 2
1.2 The Rayleigh-Plesset equation 2
1.3 Motivation for the special assignment 3

2 Numerical methods **4**
2.1 Formulation of the R-P equation 4
2.2 Fourier expansion of the pressure function 6
2.3 Numerical integration of stiff ODE's 7
2.4 Optimization of the pressure function 8

3 Results **10**
3.1 Inserting an arbitrary pressure function 10
3.2 Simple optimization tasks 10
3.3 Higher modes of driving 10

4 Summary **12**

5 Conclusion **12**

6 References **14**

1 Introduction

1.1 Sonoluminescence

The remarkable discovery that oscillating air bubbles in water can emit light has ignited widespread interest in sonoluminescence (SL), especially after the beginning of the 90's discovery by Gaitan [1] of single-bubble sonoluminescence (SBSL), which allowed the experimental parameters to be easily controlled. Under certain conditions the acoustic energy of the driving ultrasonic sound field is converted into light through the highly non-linear oscillations of the cavitating bubble. The physical conditions needed for light to arise through bubble mechanics are very extreme and studies made on the subject during the last ten years have reported bubble temperatures in the order of 25 000 – 100 000 K, pressures reaching millions of athmospheres and pulse widths of less than 100 ps [2].

The SBSL bubble is assumed to consist mainly of a noble gas [3, 4] which concentrates inside the bubble before it begins to emit light. The bubble oscillates several tens of thousands times a seconds in sync with the driving sound field and emits a short pulse of light every cycle. During the rarefaction phase of the driving pressure the bubble grows to about ten times its equilibrium radius. The compression phase causes the bubble to undergo a very rapid collapse. At the first stage of the collapse the bubble heats up adiabatically (Fig. 1a). When the bubble wall reaches supersonic speeds, shock waves are launched towards the center (Fig. 1b) where they focus and heat the interior further. The shock waves reach the center and reflect (Fig. 1c) heating the bubble to temperatures high enough for the bubble to emit a short pulse of light (Fig. 1d).

To the best of our knowledge the light is radiation from cool dense plasma but several different light emitting mechanisms have been proposed. The experimental data fits both 100 000 K black body radiation and 25 000 K bremsstrahlung radiation [5]. Recombination radiation of electrons with ions or molecular radicals has also been proposed but probably only plays a significant role in multibubble sonoluminescence (MBSL) where the temperatures reached are significantly lower. MBSL is similar as a phenomenon to SBSL but they are different in the number of bubbles and the stability of SL, and even the corresponding spectra are different [6]. The significance of shock waves to SBSL depends on the sphericity of the collapse and it is assumed that shock waves are important in SBSL but probably not in the more transient MBSL. Some papers also question the necessity of shock waves for SBSL [7].

1.2 The Rayleigh-Plesset equation

Although the short 10^{-8} s phase where the bubble emits light still partly remains a mystery the rest $4 \cdot 10^{-5}$ s of bubble dynamics during one cycle are

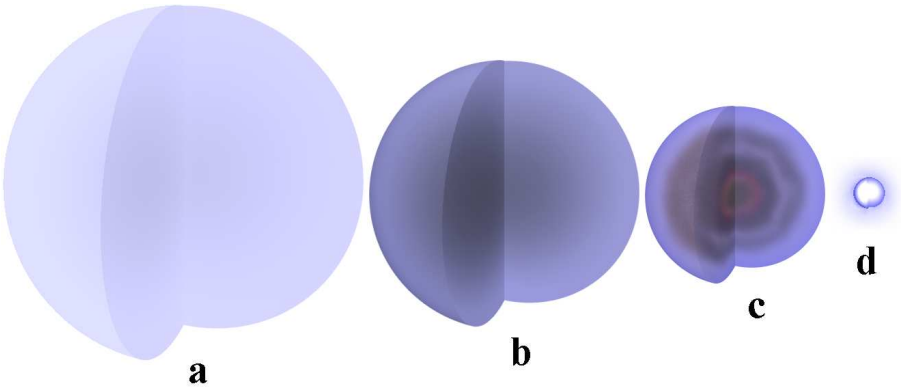

Figure 1: According to the most accepted model the sonoluminescence bubble heats up in stages. In the first phase of the compression the bubble heats up adiabatically (a–b). The supersonic implosion of the bubble walls launches shock waves towards the bubble center. The shock front focuses and heats the bubble interior further (c). In the last phase the bubble has been compressed almost down to the solid core (van der Wals hard core). The shock waves exploding outwards heat the bubble to temperatures of tens of thousands of Kelvins, and the bubble emits a short burst of light in the visible spectrum (d).

known to be well described by the non-linear Rayleigh-Plesset type equation (1). The original formulation was made by Lord Rayleigh who studied the deteoration of ship propellers on an assignment from the Royal Navy [8]. His conclusion was that the deteoration was caused by small cavitating bubbles on the propeller surfaces which could cause local pressure amplitudes of nearly gigapascals. This equation, which is based on the well-known Navier-Stokes equations of liquid dynamics, has later been refined with the effects of liquid viscosity and surface tension.

1.3 Motivation for the special assignment

Traditionally SBSL has been created with a single sine wave as the driving pressure function. However, theoretical studies suggest [9] that a nonlinear driving pressure function would be better suited for driving the itself non-linear motion of an SBSL bubble. At best, this could result in the increase of luminosity of several hundreds of percents. It has also been proposed that lowering the frequencies used in resonators could uspcale SBSL [10], although some recent studies seem to prohibit such behaviour.

In this special assignment we will construct a program for numerically solving the Rayleigh-Plesset type equation (1) with practically arbitrary driving pressure functions and freely adjustable experimental parameters.

This is hoped to facilitate the ongoing experimental SBSL studies at the laboratory and also to verify theoretically studies made on the subject of boosting SBSL [9, 10]. The intensity of sonoluminescence is known to depend on the violence of the collapse and the stability of the bubble. The former is well reflected by the quotient of minimum radius to equilibrium radius R/R_0 and we shall use this property to optimize the driving pressure function under the boundary condition of constant power. The stability of the bubble is a matter of experimental parameters and very involved theoretical calculations, so it will be out of the scope of this assignment.

2 Numerical methods

2.1 Formulation of the R-P equation

Before we can start any numerical calculation of a differential equation we have to write it into a proper form for the algorithms that we use. This is usually a set of first order differential equations with the variables chosen in an appropriate way. We shall start with the equation [11]

$$R\ddot{R}(1-\frac{2\dot{R}}{c})+\frac{3}{2}\dot{R}^2(1-\frac{4}{3}\frac{\dot{R}}{c})=\frac{R}{\rho c}\frac{dP_l(R,t)}{dt}-\frac{R}{\rho c}\frac{dP_a(0,t)}{dt} +\frac{P_l(R,t)}{\rho}-\frac{P_a(0,t)}{\rho}-\frac{P_0}{\rho}, \quad (1)$$

which differs slightly from the original Rayleigh-Plesset formulation. Here R is the bubble radius and $\dot{R}$ and $\ddot{R}$ are the first and second time (t) derivatives, respectively. ρ is the liquid density and c the speed of sound in the liquid. P_0 is the ambient pressure. The liquid pressure on the bubble surface P_l can be written [11] in the form

$$P_l(R,t)=(P_0+\frac{2\sigma}{R_0})\frac{({R_0}^3-a^3)^\gamma}{(R^3-a^3)^\gamma}-\frac{4\eta\dot{R}}{R}-\frac{2\sigma}{R}, \quad (2)$$

where the effects of surface tension σ and liquid viscosity η have been taken into account. The finite volume of the gas molecules is accounted for through the van der Wals equation of state, where a is the van der Wals hard core. For adiabatic change $pV^\gamma = const$, with γ the ratio of specific heats (adiabatic constant) and R_0 the equilibrium radius of the bubble. The respective total time derivate now becomes

$$\frac{dP_l(R,t)}{dt}=(P_0+\frac{2\sigma}{R_0})\frac{({R_0}^3-a^3)^\gamma}{(R^3-a^3)^{\gamma+1}}\cdot(-3\gamma)R^2\dot{R}+\frac{4\eta\dot{R}^2}{R^2}+\frac{2\sigma\dot{R}}{R^2}-[4\eta\frac{\ddot{R}}{R}]^*. \quad (3)$$

The term $-4\eta\frac{\ddot{R}}{R}$ depends explicitly on $\frac{\partial\dot{R}}{\partial t}$ and should therefore be moved to the left-hand side of equation (7). To simplify following calculations $\frac{\partial\dot{R}}{\partial t}$

will be solved out explicitly and $\frac{dP_l(R,t)}{dt}$ henceforth *defined* without the last term marked with '*'. If we assume that the number of gas molecules in the bubble remains constant during the collapse we can write for the smallest possible radius [11]

$$a = \frac{R_0 \cdot 2.3}{20}. \tag{4}$$

For the purposes of our numerical calculations the sound field pressure (ambient pressure amplitude) P_a will be given in the form of a finite sine series

$$P_a(0,t) = |P_a| \sum_{n=0}^{N} A_n \sin(n\omega t + \phi_n), \qquad \sum_{n=0}^{N} A_n^2 = 1, \tag{5}$$

which is easily derivated with respect to time. The square sum, or norm, for A_n is needed to keep the power of the pressure field constant. The equation (1) is rewritten as a set of two first order differential equations

$$\frac{\partial}{\partial t} R = \dot{R}, \tag{6}$$

$$\frac{\partial}{\partial t} \dot{R} = \frac{-\frac{3}{2}\dot{R}^2(1 - \frac{4}{3}\frac{\dot{R}}{c}) + \frac{R}{\rho c}(\frac{dP_l(R,t)}{dt} - \frac{dP_a(0,t)}{dt}) + \frac{P_l(R,t)}{\rho} - \frac{P_a(0,t)}{\rho} - \frac{P_0}{\rho}}{R(1 - \frac{2\dot{R}}{c}) + \frac{4\eta}{\rho c}}. \tag{7}$$

The second term in the denominator comes from equation (3) when $\ddot{R}$ is solved out. Therefore $\frac{dP_l(R,t)}{dt}$ is defined in such a way that it has no explicit dependence on $\ddot{R}$. For our algorithms we also need to solve analytically the Jacobian matrix of the set differential equations (6,7)

$$\mathbf{J} = \begin{bmatrix} \frac{\partial F_1}{\partial R} & \frac{\partial F_1}{\partial \dot{R}} & \frac{\partial F_1}{\partial t} \\ \frac{\partial F_2}{\partial R} & \frac{\partial F_2}{\partial \dot{R}} & \frac{\partial F_2}{\partial t} \end{bmatrix}, \tag{8}$$

where F_1 and F_2 are the right-hand sides of equations (6) and (7) respectively.

The partial derivations are straight-forward but rather tedious operations, which result in the equations (9–22).

$$\frac{\partial F_1}{\partial R} = 0, \tag{9}$$

$$\frac{\partial F_1}{\partial \dot{R}} = 1, \tag{10}$$

$$\frac{\partial F_1}{\partial t} = 0, \tag{11}$$

$$\frac{\partial F_2}{\partial R} = \frac{\frac{\partial f}{\partial R} g - f \frac{\partial g}{\partial R}}{g^2}, \tag{12}$$

$$\frac{\partial F_2}{\partial \dot{R}} = \frac{\frac{\partial f}{\partial \dot{R}} g - f \frac{\partial g}{\partial \dot{R}}}{g^2}, \tag{13}$$

$$\frac{\partial F_2}{\partial t} = \frac{R}{\rho c}\frac{d^2 P_a(0,t)}{dt^2} - \frac{dP_a(0,t)}{\rho}, \tag{14}$$

where f and g are the numerator and denominator of the right-hand side of equation (7) i.e. F_2. Note that $P_l(R,t)$ doesn't depend explicitly on time whereas $P_a(0,t)$ does.

When the partial derivatives of f and g are evaluated we get

$$\frac{\partial f}{\partial R} = \frac{1}{\rho c}\left(\frac{dP_l(R,t)}{dt} - \frac{dP_a(0,t)}{dt}\right) + \frac{R}{\rho c}\frac{\partial dP_l(R,t)}{\partial R dt} + \frac{1}{\rho}\frac{\partial P_l(R,t)}{\partial R}, \quad (15)$$

$$\frac{\partial f}{\partial \dot{R}} = -3\dot{R}(1-2\frac{\dot{R}}{c}) + \frac{R}{\rho c}\frac{\partial dP_l(R,t)}{\partial \dot{R} dt} + \frac{1}{\rho}\frac{\partial P_l(R,t)}{\partial \dot{R}}, \quad (16)$$

$$\frac{\partial g}{\partial R} = 1 - \frac{2\dot{R}}{c}, \quad (17)$$

$$\frac{\partial g}{\partial \dot{R}} = -\frac{2R}{c}, \quad (18)$$

with partial derivatives $\frac{\partial P_l(R,t)}{\partial R}$, $\frac{\partial P_l(R,t)}{\partial \dot{R}}$ and $\frac{\partial dP_l(R,t)}{\partial R dt}$, $\frac{\partial dP_l(R,t)}{\partial \dot{R} dt}$ being

$$\frac{\partial P_l(R,t)}{\partial R} = (P_0 + \frac{2\sigma}{R_0})\frac{({R_0}^3 - a^3)^\gamma}{(R^3-a^3)^{\gamma+1}}\cdot(-3\gamma)R^2 + \frac{4\eta\dot{R}}{R^2} + \frac{2\sigma}{R^2}, \quad (19)$$

$$\frac{\partial P_l(R,t)}{\partial \dot{R}} = -\frac{4\eta}{R}, \quad (20)$$

$$\frac{\partial dP_l(R,t)}{\partial R dt} = (P_0 + \frac{2\sigma}{R_0})\frac{({R_0}^3 - a^3)^\gamma}{(R^3-a^3)^{\gamma+1}}\cdot(-3\gamma)R\dot{R}\left(2 - \frac{3(\gamma+1)R^3}{(R^3-a^3)}\right) - \frac{8\eta\dot{R}^2}{R^3} - \frac{4\sigma\dot{R}}{R^3}, \quad (21)$$

$$\frac{\partial dP_l(R,t)}{\partial \dot{R} dt} = (P_0 + \frac{2\sigma}{R_0})\frac{({R_0}^3 - a^3)^\gamma}{(R^3-a^3)^{\gamma+1}}\cdot(-3\gamma)R^2 + \frac{8\eta\dot{R}}{R^2} + \frac{2\sigma}{R^2}. \quad (22)$$

Now, combining equations (2-22) we have a full description of the non-linear differential equations needed for our program.

2.2 Fourier expansion of the pressure function

In the last subsection we saw that the pressure function $P_a(0,t)$, or ambient pressure amplitude, was chosen to be presented as a Fourier sine series with a phase factor ϕ_n. The reasons for this were mainly practical: if the pressure function and its time derivatives can be presented in a simple analytical form, no numerical derivation will be needed and the computation is generally faster. With a sufficiently large number of terms (say $N \approx 200$) any reasonably well-behaved function can be presented as a Fourier series with good accuracy. But more importantly, we will later need to expand the pressure function in some basis for the purpose of optimization. For this, Fourier sine series is as good as any and saves us the trouble of converting the basis between the optimizer and the integrator routines. As

an additional bonus, comparison of the optimized pressure function to the traditional choice, $\sin(\omega t)$, becomes very straightforward.

An arbitrary pressure function (in a vector form) can be expanded into a Fourier sine series with N terms using discrete Fourier transform (DFT) [12],

$$X(k) = \Sigma_{n=1}^{N} x(n) e^{-j2\pi i(k-1)(n-1)/N}, 1 \leq k \leq N. \tag{23}$$

The relationship between DFT and the Fourier coefficients a and b in

$$x(n) = a_0 + \Sigma_{k=1}^{N/2} a(k)\cos(2\pi kt(n)/(Ndt)) + b(k)\sin(2\pi kt(n)/(Ndt)) \tag{24}$$

is

$$\begin{aligned} a_0 &= X(1)/N, \\ a(k) &= 2Re(X(k+1))/N, \\ b(k) &= -2Im(X(k+1))/N, \end{aligned} \tag{25}$$

where x is a length N discrete signal sampled at times t with spacing dt. The Fourier series can be finally rewritten as a sine series using relation

$$\begin{aligned} \sin(nt + \phi_n) &= \sin(\phi_n)\cos(nx) + \cos(\phi_n)\sin(nx) \\ &= a_n \cos(nx) + b_n \sin(nx), \end{aligned} \tag{26}$$

which can be used to solve

$$\phi_n = \arctan(\frac{a_n}{b_n}). \tag{27}$$

2.3 Numerical integration of stiff ODE's

The major challenge in numerically integrating the set of ordinary differential equations (ODE's) obtained in last subsection are the very different time scales involved. The oscillations generally take place at time scales of millisecons and speeds of few meters per second but near the collapse the time scale reduces to nanoseconds and speeds exceed 1000 m/s. To obtain numerically valid results (relative errors less than perhaps 0.1 %) with a reasonable amount of computation time one needs an integrator capable of reducing the step size near the time of collapse, taking longer steps where possible.

ODE's involving such drastic changes in their time behaviour are known as stiff. The *Numerical Recipes in C* (NRC) [13] discusses several suitable algorithms, from which stiff and stifbs were chosen for experimenting. Stiff uses a fourth order Rosenbrock method, which is a generalization of the Runge-Kutta method with an embedded automatic stepsize adjustment. The potentially faster method stifbs uses a semi-implicit extrapolation method which is a modification of the Burlisch-Stoer method.

Both algorithms were tried out with realistic SL parameters, and it was found that stifbs often failed in integration because it tried to calculate values with $R < a$, which leads to an error when γ is not an integer (as it generally isn't), not to mention it being physically impossible. NRC states that stifbs is intended smooth functions and is not particularly good for differential equations with singular points *inside* the domain of integration. Apparently the van der Wals hardcore $R = a$ counts as one. On the other hand, Runge-Kutta methods such as stiff with adaptive stepsize control are known to do an excellent job in feeling their way through rocky and discontinuous terrain. Therefore, stiff was chosen for the integration routine. For moderate accuracies ($\epsilon \leq 10^{-4} - 10^{-5}$ in the error criterion) and moderate-sized systems ($N \leq 10$) stiff is competitive with more complicated algorithms like stifbs. With more stringent parameters stiff still remains reliable, merely becomes less efficient. The parameter set for stiff was chosen to be that by Shampine, see [13] for other alternatives.

2.4 Optimization of the pressure function

Before we can start any optimization, we have to first decide what is the goal of optimization and what are the parameters that can be changed. In this case the goal would be more robust sonoluminescence. This itself is difficult to determine since we can only use information about the time dependence of the bubble radius so we need some auxiliary variable that depends monotonically on the robustness of SL. Suitable variables could be e.g. temperature at the time of collapse (for this we could use some equation relating pressure and volume to temperature), the ratio R_{max}/R_{min} or the ratio R_{min}/R_0 (αR_{min}, when $R_0 = const$). None of these can be used to directly determine the amount of increase in the intensity of SL unless we can determine the exact relation between them and the robustness of SL. However, the requirement of monotonicity is enough to assure that optimization gives the same point in parameter space as it would with optimizing the intensity or robustness of SL. Following the example of earlier studies [9], R_min was chosen as the indicator of the most violent collapse, and thus, of the most intense SL.

The parameter space is the pressure function itself. For a realistic pressure function we can safely assume that the function is both continuous and reasonably well-behaved. To reduce the amount of parameters to a manageable number we can expand the function as a sum in some suitably quickly converging basis, taking only a finite number of terms. In this special assignment the basis was chosen to be a finite Fourier sine series

$$P_a(t) \approx \Sigma_{n=1}^{N} P_n \sin(n\omega t + \phi_n). \tag{28}$$

This choice has the distinct advantage that the discrete Fourier transform of the pressure function can be very easily calculated from the pressure

coefficients P_n and phases ϕ_n. Also, the first term, $\sin(\omega t)$, is exactly the pressure function used in perhaps 99% of SL experiments, and thus the optimized results can be easily compared to reality.

Next, a suitable algorithm needs to be chosen. Requirements are that the algorithm is preferably quick but more importantly, that it is able to explore all the possible local minima in parameter space efficiently. Very little is known about the shape of the objective function beforehand, so it is difficult to make a guess about a reasonable starting point or the shape or position of any local minima. For this reason, and relying on the experience of other researchers [9], the algorithm amebsa [13] was chosen for the task.

Amebsa is essentially a heuristic algorithm based on simulated annealing. It starts by randomly guessing $N + 1$ starting points, or vertices in the simplex, where N is the number of parameters to be optimized. Values of the objective function are calculated for each vertex. The vertices are then approximately randomly moved in the parameter space, within a region relative to the current temperature and the energy, or objective function value, of the nearby points. To keep the power $(\Sigma|P_n|^2)$ of the pressure function constant, each P_n is normalized by $P_0 \cdot \Sigma_{n=1}^{N}|P_n|^2$ after every random step.

To make a connection with thermodynamics, the simplex expands to a size that can be reached at the current temperature, and then executes a stochastic, tumbling Brownian motion within that region, sampling new, approximately random, points as it does so. If the temperature is reduced slowly enough, it becomes highly likely that the simplex will shrink into the region containing the lowest relative minimum. This is exactly what happens when liquids freeze and crystallize or metals slowly cool and anneal, and what gives the name simulated annealing for the method.

The crucial point is in determining the suitable annealing schedule, i.e. how long new points are sampled in a certain temperature and how much temperature is reduced each time. Restarts, where one vertex is replaced by the best point encountered so far, can also have very positive effect depending on the problem, although sometimes the effect can also be slightly negative. The following four schedules [13] have been included in the optimization program:

- Reduce T to (1-ϵ)T after every m moves, where ϵ/m is determined by experiment.

- Budget a total of K moves, and reduce T after every m moves to a value $T = T_0(1 - k/K)^\alpha$, where k is the cumulative number of moves thus far, and α is a constant, say 1, 2, or 4. The optimal value for α depends on the statistical distribution of relative minima of various depths. Larger values of α spend more iterations at lower temperature.

- After every m moves, set T to β times $f_1 - f_b$, where β is and exper-

imentally determined constant of order 1, f_1 is the smallest function value currently represented in the simplex, and f_b is the best function ever encountered. However, never reduce T by more than some fraction γ at a time.

The most commonly used schedule in this special assignment has been schedule 1, reducing the temperature by a constant fraction, although other schedules seem to give similar results.

3 Results

The computations in this special assignment were performed with a program tailored for the job, *Sonodiff*. A more detailed description of the program or a "user's manual" is supplied as a separate appendix, including also listings of the source code or references to the appropriate pages of *Numerical Recipes in C*.

3.1 Inserting an arbitrary pressure function

The R-P equation was first solved numerically using a simple sine wave pressure function and parameters listed in Table 1, see Fig. 2. Having obtained both qualitatively and quantitatively reasonable results, the pressure function editor was next tested with square and triangle wavefunctions created by Matlab, see Fig. 5 and Fig. 6, as well as with some other functions. The Matlab functions were first Fourier transformed with Matlab's discrete Fourier transform (DFT) and typed in the editor. The editor calculated the 200-term Fourier sine series using equation 23. The qualitative results seem to verify that the pressure function editor works properly.

3.2 Simple optimization tasks

The optimization algorithm was first used to reproduce results in earlier articles [9] for bimodal driving: The R-P equations differ in some parts, e.g. liquid compressibility is neglected in the model used in this assignment and some parameters are slightly different. Fig. 7 and Fig. 8 show the graphs drawn for the optimized bimodal driving and the pressure function from literature, respectively, and with the same set of parameters (Table 1). Fig. 3 shows the same graphs superimposed for easy comparison.

3.3 Higher modes of driving

Finally, the optimizing code was used to calculate higher orders of driving. Figures 9 and 10 show 8-mode and 16-mode driving. A comparison of the results with the corresponding pressure function can be seen in Fig. 4. It should be noted that convergence in the pressure function with these higher

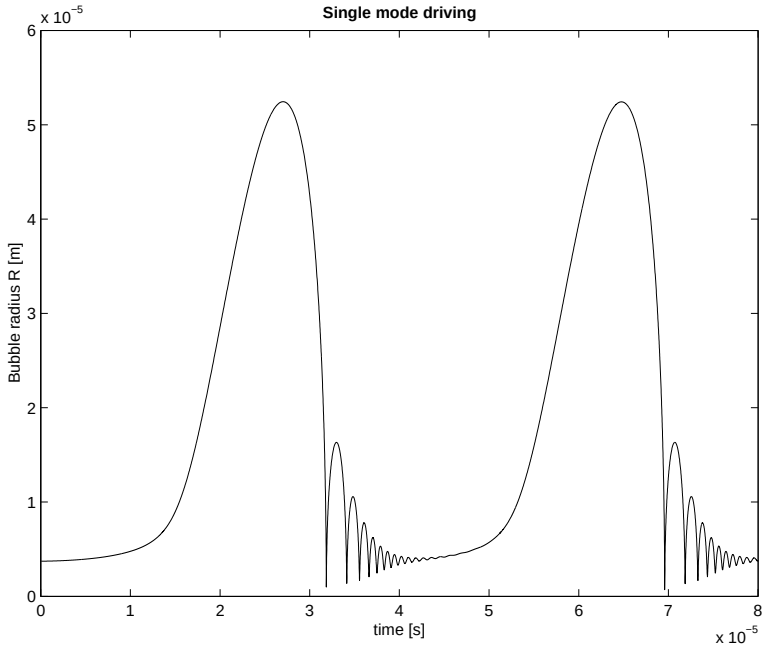

Figure 2: $R(t)$ curve obtained using the classical single mode driving.

modes was relatively weak because the code isn't especially efficient at the moment. As such, the number of iterations at each temperature had to be limited to a quite small value (around $2N$), which is generally too small to obtain good convergence to the optimum value. Nevertheless, each higher mode showed results superior to the previous modes. Table 2 summarizes the results for different modes of driving.

Default values

$c = 1.481 \cdot 10^3$ m/s	C	Speed of sound in the liquid
$\rho = 1.000 \cdot 10^3$ kg/m^3	RHO	Density of the liquid
$\omega = 1.665 \cdot 10^5$	W	Frequency of ambient pressure in rads, 26.5 kHz$\cdot 2\pi$
$P_a = 1.350 \cdot 10^5$ Pa	APA	Maximum value of ambient pressure, 1.35 bar
$P_0 = 1.000 \cdot 10^5$ Pa	P0	External pressure, 1 bar
$\sigma = 3.000 \cdot 10^{-2}$ kg/s^2	SG	Surface tension of the liquid
$R_0 = 4.500 \cdot 10^{-6}$ m	R0	Equilibrium radius of the bubble
$A = 5.175 \cdot 10^{-7}$ m	A	Van der Wals hard core, $2.3/20 \cdot R_0$
$\gamma = 1.4000$	GM	Ratio of specific heats for a diatomic gas
$\eta = 3.00 \cdot 10^{-3}$ kg/ms	ETA	Viscosity of the gas

Table 1: Values used for the experimental parameters.

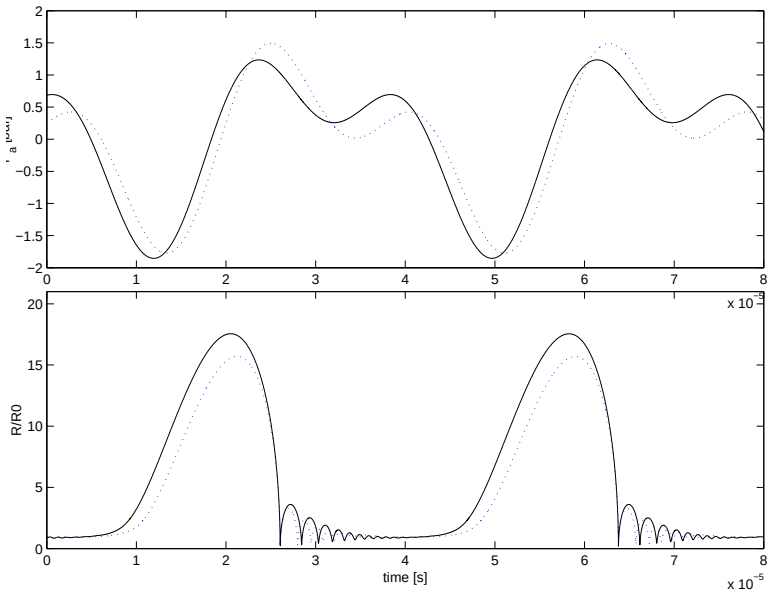

Figure 3: Bimodal driving optimized using Sonodiff (solid) and with parameters from literature (dashed) [9] compared.

4 Summary

This special assignment focused on the numerical modeling and optimization of the Rayleigh-Plesset equations that govern the behaviour of a sonoluminescing or in general, cavitating bubble. We first rewrote the R-P equation in the form that is the most compatible with most numerical algorithms, a set of first order ordinary differential equations. Next, we wrote a program that can integrate the set of (stiff) first order R-P equations using an adaptive stepsize control. The program was written to take all parameters and the driving pressure function as input.

Heuristical optimization algorithms were then added to optimize the bubble behaviour using a pressure function expanded as a Fourier sine series. The program was first tested without optimization and using simple pressure functions. Next, bimodal driving was optimized and the results compared to ones obtained previously [9]. Finally, also higher modes of driving up to 16-mode were optimized.

5 Conclusion

This special assignment is hoped to facilitate the future sonoluminescence projects at the Materials Physics Laboratory at the Helsinki University of Technology. In previous projects at the laboratory we have established a fully working close experimental sonoluminescence setup [14, 15, 16, 17, 18].

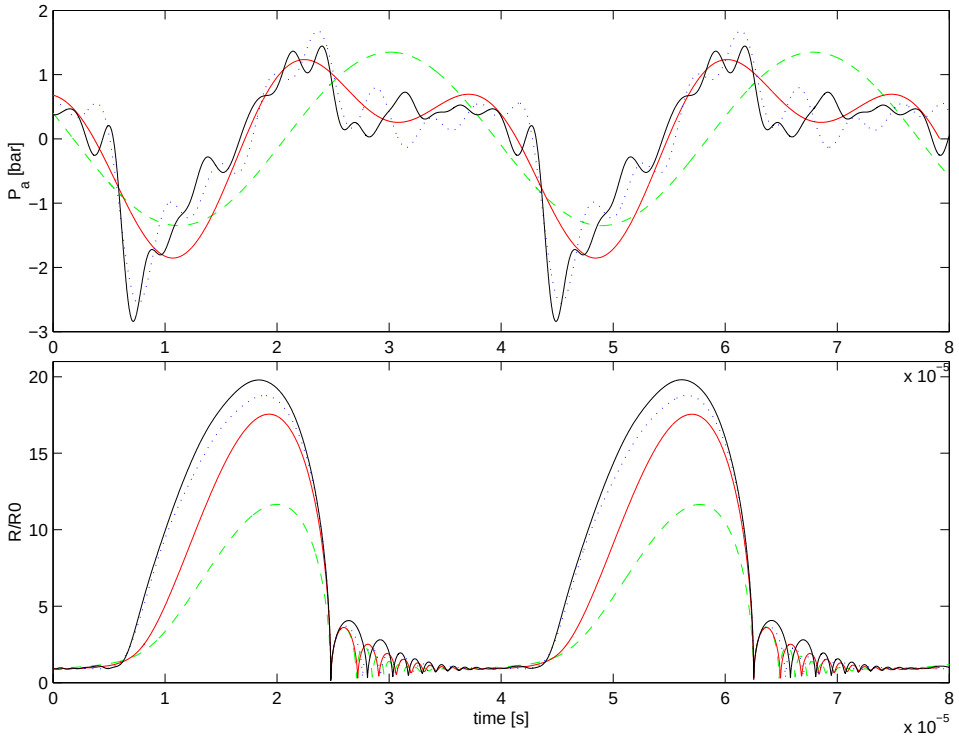

Figure 4: Results for single mode (dashed) and multimodal driving (bimodal solid, eightmode dotted, sixteenmode solid) shown on the same scale.

Another parallel project has theoretically studied the dependence of the Mie scattering intensity on the bubble radius [19]. It is hoped that these theoretical efforts will be soon combined with experiment to give us the ability to study and control the time behaviour of the radius of a sonoluminescing bubble.

Later experiments will hopefully reveal how well the approximations made in the formulation of the R-P equation hold. It might be useful to include the effects of finite liquid compressibility, shock wave formation and shedding etc. to the model but this will be determined by experiment alone. Later experimental progress will also show whether the optimized pressure functions presented here will be feasible in reality.

Optimization results

Mode	R_{min} [μm] / $\lvert\dot{R}_{max}\rvert$ [m/s]	n: A_n, ϕ_n
singlemode	0.697 / 427	1: 1, 0
bimodal (Sonodiff)	0.602 / 886	1: 0.8142, -2.110 2: 0.5806, 3.107
bimodal [9]	0.610 / 812	1: 0.7894, 2.9042 2: 0.6139, 0.0000
eightmode	0.594 / 980	1: 0.7302, 1.625 2: 0.5157, -2.287 3: 0.1762, 2.326 4: 0.2551, -0.7720 5: 0.1065, 3.247 6: 0.1801, -0.07764 7: 0.05775, -1.899 8: 0.2401, -0.3247
sixteenmode	0.592 / 1000	

Table 2: Results for different modes of driving and the corresponding amplitudes and phases.

6

References

[1] D. F. Gaitan, L. A. Crum, C. C. Church, and R. A. Roy, J. Acoust. Soc. Am. **91**, 3166 (1992).

[2] B.P. Barber, R.A. Hiller, R. Löfstedt, S.J. Putterman, and K.R. Weninger, "Defining the Unknowns of Sonoluminescence", *Phys. Rep.* **281**, 65 (1997).

[3] D. Lohse, M.P. Brenner, T.F. Dupont, S. Hilfgenfeldt, and B. Johnston, "Sonoluminescing Air Bubbles Rectify Argon", *Phys. Rev. Lett.* **78**, 1359 (1997).

[4] D. Lohse and S. Hifgenfeldt, "Inert Gas Accumulation in Sonoluminescing Bubbles", *J. Chem. Phys.* **107**, 6986 (1997).

[5] R. Hiller, S.J. Putterman, and B.P. Barber, "Spectrum of Synchronous Picosecond Sonoluminescence", *Phys. Rev. Lett.* **69**, 1182 (1992).

[6] T.K. Matula, R.A. Roy, P.D. Mourad, W.B. McNamara III, and K.S. Suslick, "Comparison of Multibubble and Single-Bubble Sonoluminescence Spectra", *Phys. Rev. Lett.* **75**, 2602 (1995).

[7] H.Y. Cheng, M.-C. Chu, P.T. Leung, and L. Yuan, "How important are shock waves to single-bubble sonoluminescence?", *Phys. Rev. E*, **58**, R2705 (1998).

[8] Lord Rayleigh, "On the Pressure Developed in a Liquid on the Collapse of a Spherical Cavity", *Phil. Mag.* **34**, 94 (1917).

[9] J. Holzfuss, M. Rüggeberg, adnd R. Mettin, "Boosting Sonoluminescence", *Phys. Rev. Lett.* **81**, 1961 (1998).

[10] S. Hilgenfeldt, D. Lohse "Predictions for Upscaling Sonoluminescence", *Phys. Rev. Lett.* **82**, 1036 (1999).

[11] B.P. Barber, "Synchronous picosecond sonoluminescence", *Ph.D. thesis*, UCLA (1992).

[12] Matlab help. Matlab's internal command *FFT* was used for discrete Fourier transforms.

[13] W.H. Press, S.A. Teukolsky, W.T. Vetterling, B.P. Flannery, "Numerical Recipes in C", 2nd Edition, Cambridge University Press (1995).

[14] A. Särkilahti, "Sonoluminescence", Special Assignment, Materials Physics Laboratory, HUT (1996).

[15] A. Särkilahti, "Nesteen kaasupitoisuuden kontrolloiminen suljetussa sonoluminesenssilaitteistossa", Special Assignment, Advanced Energy Systems, HUT.

[16] A. Särkilahti, "Single-Bubble Sonoluminescence", Master's Thesis, Materials Physics Laboratory, HUT (2000).

[17] T. J. Mäki, "Suljetun sonoluminesenssilaitteiston rakentaminen", Special Assignment, Materials Physics Laboratory, HUT (2000).

[18] M. A. Voutilainen, "Sonoluminesenssilaitteiston parametrit ja niiden määritys", Materials Physics Laboratory, HUT (2000).

[19] V. A. Bergholm, "Mie-sironta kuplasta", Materials Physics Laboratory, HUT (2002).

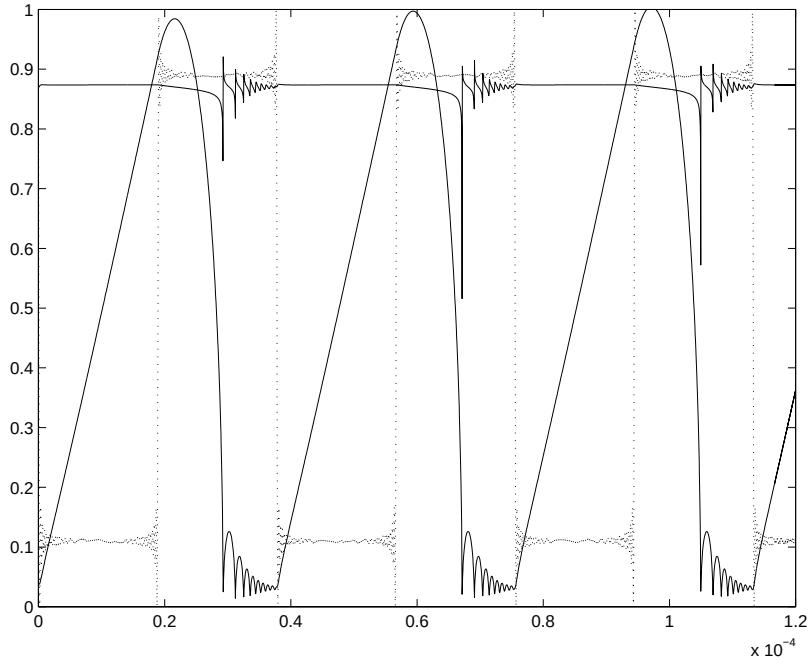

Figure 5: $R(t)$ and $\dot{R}(t)$ curves (solid) for square pressure function (dotted).

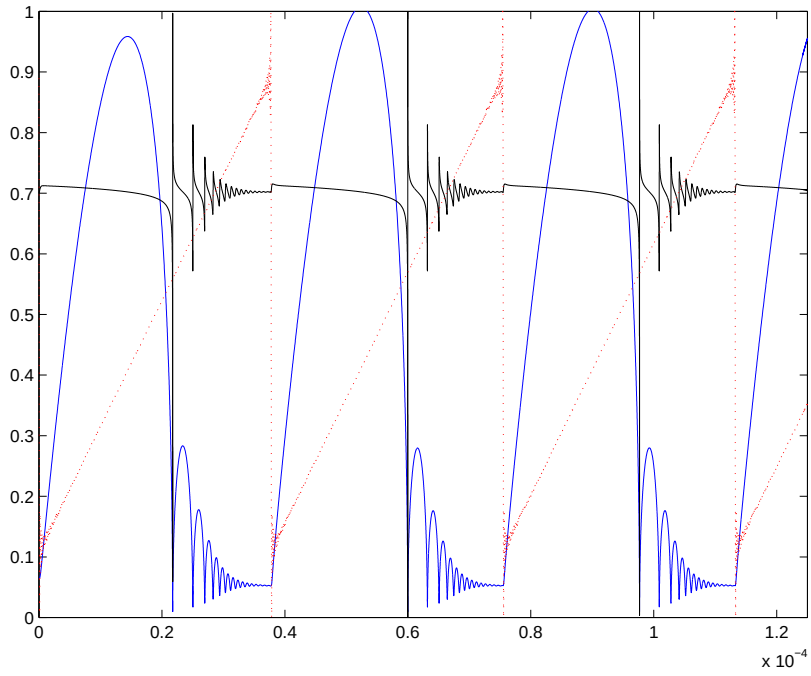

Figure 6: $R(t)$ and $\dot{R}(t)$ curves (solid) for sawtooth pressure function (dotted).

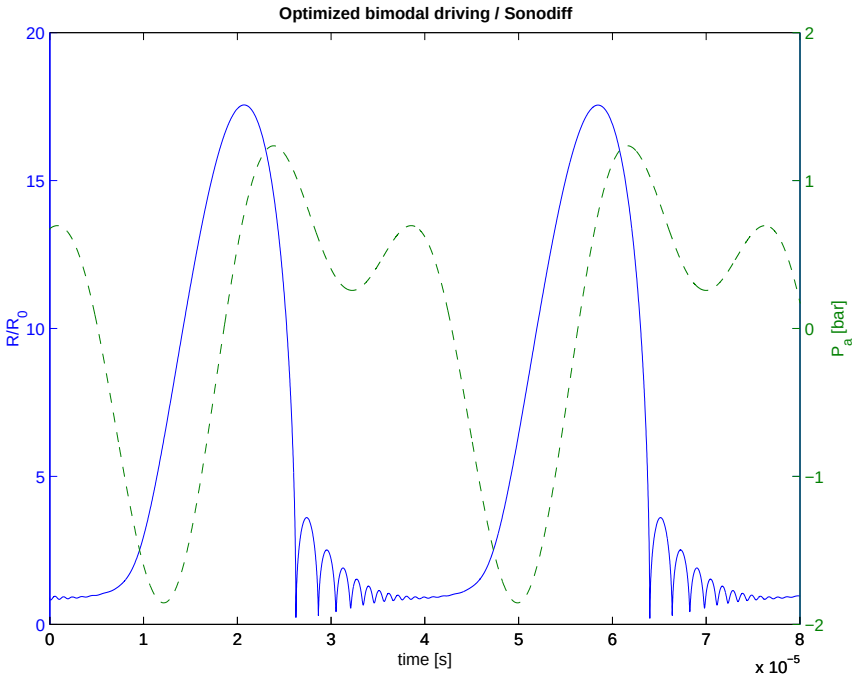

Figure 7: Bimodal driving optimized using Sonodiff.

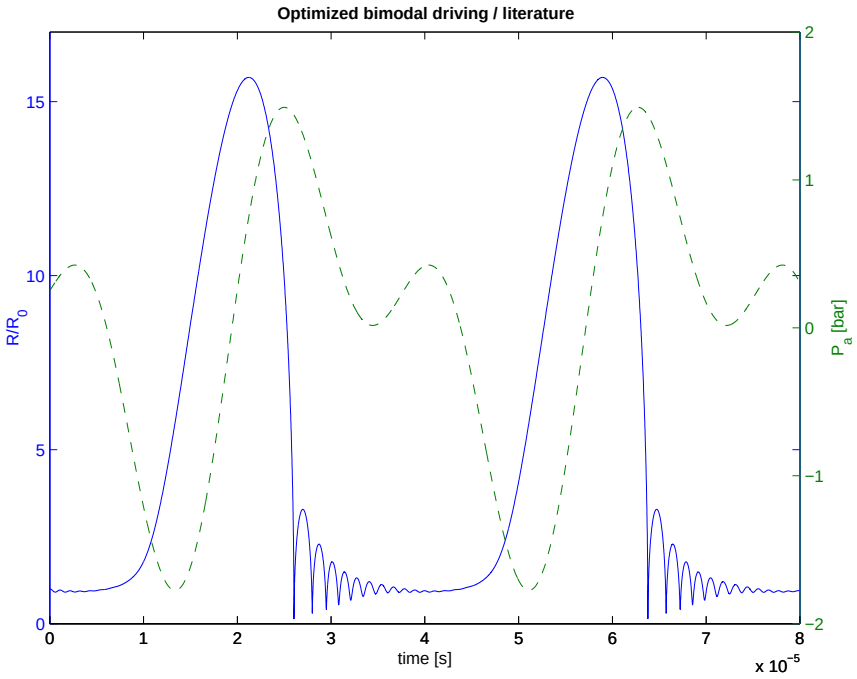

Figure 8: Bimodal driving using pressure functio parameters from literature [9].

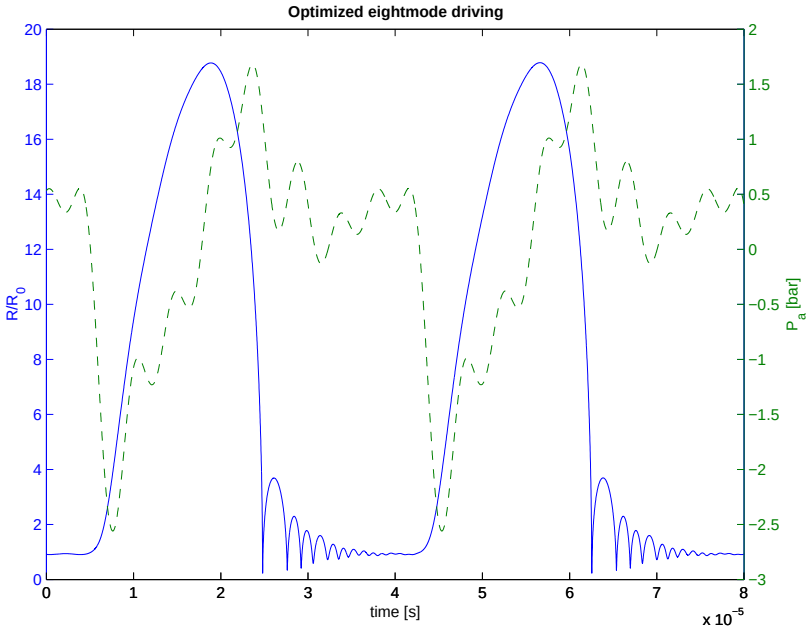

Figure 9: Eightmode driving.

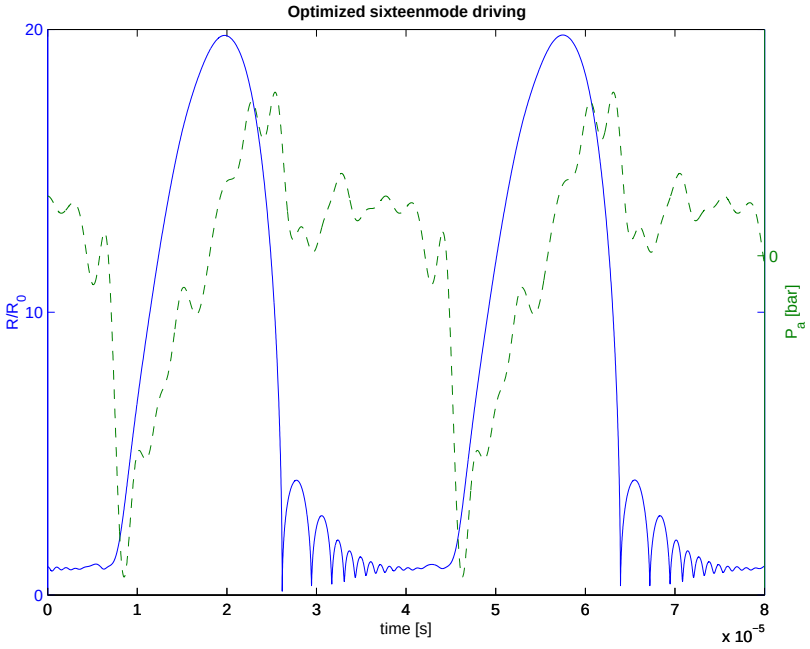

Figure 10: Sixteenmode driving.